High-spin structures in the ^{129}Xe nucleus

Y. Huang,[1] Z. G. Xiao,[1,2,*] S. J. Zhu,[1] C. Qi,[3] Q. Xu,[4] W. J. Cheng,[1] H. J. Li,[1] L. M. Lyu,[1] R. S. Wang,[1] W. H. Yan,[1] H. Yi,[1] Y. Zhang,[1] Q. M. Chen,[5] C. Y. He,[5] S. P. Hu,[5] C. B. Li,[5] H. W. Li,[5] P. W. Luo,[5] X. G. Wu,[5] Y. H. Wu,[5] Y. Zheng,[5] and J. Zhong[5]

[1]*Department of Physics, Tsinghua University, Beijing 100084, China*

[2]*Collaborative Innovation Center of Quantum Matter, Beijing 100084, China*

[3]*Department of Physics, Royal Institute of Technology, SE-10691 Stockholm, Sweden*

[4]*College of Physics and Optoelectronics, TaiYuan University of Technology, TaiYuan 030024, China*

[5]*China Institute of Atomic Energy, Beijing 102413, China*

(Received 11 December 2015; published 13 June 2016)

High-spin states in the ^{129}Xe nucleus are studied with the reaction ^{124}Sn(^{9}Be,$4n$) at a beam energy of 36 MeV. The level scheme is extended significantly. For the positive-parity band, the $\alpha = +1/2$ and the $\alpha = -1/2$ signature components are combined to form a complete band structure based on the $3/2^+$ state with spin and parity up to $21/2^+$. For the negative-parity band based on the $11/2^-$ state, the $\alpha = +1/2$ signature component is newly established and both the $\alpha = +1/2$ and the $\alpha = -1/2$ signature components also form a complete band structure up to the $35/2^-$ state. The positive- and negative-parity bands are proposed to originate from $\nu d_{3/2}\, 3/2^+[402]$ and $\nu h_{11/2} 11/2^-[505]$ Nilsson configurations, respectively. A backbending is observed in the negative-parity band, which originates from the alignments of two $h_{11/2}$ protons according to crank shell model calculations. Based on the total Routhian surface and quasiparticle triaxial rotor model calculations, the negative-parity band is interpreted as a triaxially deformed shape with $\gamma \approx -30^\circ$, while the positive-parity band is associated with γ softness, in accordance with previous studies. In the high-spin states, three decoupled bands and one oblate band with $\gamma \approx -60^\circ$ are newly identified. The systematics and other characteristics of these bands are discussed.

DOI: 10.1103/PhysRevC.93.064315

I. INTRODUCTION

The abundant nuclear shapes and shape coexistence are the results of the complicated interplay between the single-particle motion and the collective motion of the nucleus as a quantum many-body system. While most deformed nuclei are of axially symmetric prolate and oblate shapes, axial asymmetry or triaxiality manifests itself in some specific mass regions due to the polarization interaction of the nucleon near the Fermi surface to a soft core, leaving the observed signals in γ bands [1,2], wobbling motions at a high angular momentum [3,4], enhanced signature splitting, or even signature inversion [5–7]. Of particular interest is the $A \approx 130$ transitional mass region, where the proton number is above the $Z = 50$ shell and the neutron number is below the $N = 82$ shell. At low spins, the nuclei show small β_2 and soft γ deformation. At high spins, shape coexistence may occur due to the competition between the proton alignment near the bottom of the $h_{11/2}$ subshell, driving the nucleus to a prolate shape, and the neutron alignment near the top of the $h_{11/2}$ subshell, driving it to an oblate shape [8], known as the deformation driving effect, as first reported in ^{131}La [9]. Moreover, the inverse driving properties of neutron and proton give rise to various shapes in different nuclei, depending on the (quasi)particle configuration. For example, oblate bands caused by this deformation driving effect have been observed in ^{131,136,137}La [9–11], ^{132}Ba [12], ^{137,138,139}Pr [13–15], ^{138}Pm [16], and ^{139}Nd [17], among others.

The odd-mass nuclei in the Xe-Ba-Ce region have been theoretically investigated systematically within the Strutinsky mean-field method based on the existing data. The increasing γ softness in combination with the deformation driving effect leads to a smooth transition from an approximately prolate shape to a triaxial or oblate shape as the neutron number N increases, where some isotopes with larger N exhibit coexisting minima on the total Routhian surface (TRS), indicating shape coexistence [8]. A similar trend was reported for even-even isotopes in the same region [18]. This deformation driving effect was recently observed in ^{128}Xe [19].

The ^{129}Xe nucleus, located in the same mass region, has been studied with regard to β^+ decay of ^{129}Cs [20,21]. Then a negative-parity band with one signature, $\alpha = -1/2$, was established to moderate spin through the ^{128}Te(α,$3n$) reaction [22]. Using the ^{130}Te(^{3}He,$4n$) and ^{126}Te(α,n) reactions, a positive-parity band was identified in addition [23]. Comparison with the particle plus core model calculations for the positive-parity band indicates a vibration type of core excitation in the positive-parity band, while the negative-parity band was reproduced in triaxial rotor model calculations. Later the level structures were updated using the same reaction, ^{126}Te(α,n), by adding numerous levels below the excitation energy of 2.5 MeV [24]. However, so far the collective band structures up to high-spin states above this energy of ^{129}Xe are still lacking compared with the other nuclei in this region.

In this paper, we present new experimental results on high-spin states in ^{129}Xe. Many new levels and transitions are identified. The results are compared with the cranked shell model calculations and the quasiparticle triaxial rotor model calculations.

*xiaozg@tsinghua.edu.cn

II. EXPERIMENT AND RESULTS

The experiment was carried out at the HI-13 Tandem Accelerator at the China Institute of Atomic Energy (CIAE). The high-spin states of ^{129}Xe were populated through the fusion-evaporation reaction ^{124}Sn(^{9}Be,$4n$) at a beam energy of 36 MeV, which was optimized after the excitation function was measured between 32 and 38 MeV. The target was an enriched ^{124}Sn of thickness 1.16 mg/cm^2 on a gold backing of thickness 3.3 mg/cm^2. Twelve Compton-suppressed HPGe detectors and one planar HPGe detector were employed to detect in-beam γ rays. The detectors were placed at angles of 40°, 90°, 120°, 140°, and 150° with respect to the beam direction. Energy and efficiency calibrations were done with a ^{133}Ba and a ^{152}Eu standard source before and after the beam time. The typical energy resolution of the HPGe detector represented by the full width at half-maximum (FWHM) of the γ peak is better than 2.0 keV for the 1332.5-keV γ ray of ^{60}Co. The residue of linear fit to the γ energies of ^{133}Ba and ^{152}Eu sources in the energy calibration is 1.0 keV on average. The total photo peak efficiency of the detector array is slightly above 0.3%. A γ-γ coincidence matrix and an asymmetry two-dimensional angular-correlation matrix were constructed to obtain the directional correlation of oriented state (DCO) ratios [25]. A total of 1.9×10^7 coincidence events were collected in the γ-γ coincidence matrix. Coincidence data were analyzed with the RADWARE software package [26].

The level scheme of ^{129}Xe obtained in the current work is presented in Fig. 1. It was deduced from the γ-γ coincidences, the relative transition intensities, and the DCO ratio analysis. A total of 31 new levels and 48 new transitions are identified. Six collective band structures and three single-particle level clusters are labeled at the top with the numbers (1)–(6) and (I)–(III), respectively. Compared with previous results [23,24], the level scheme of ^{129}Xe at high spins is extended and expanded significantly in the current work.

In a previous publication [24], the low-lying states of the positive-parity band, (1), were established with spin and

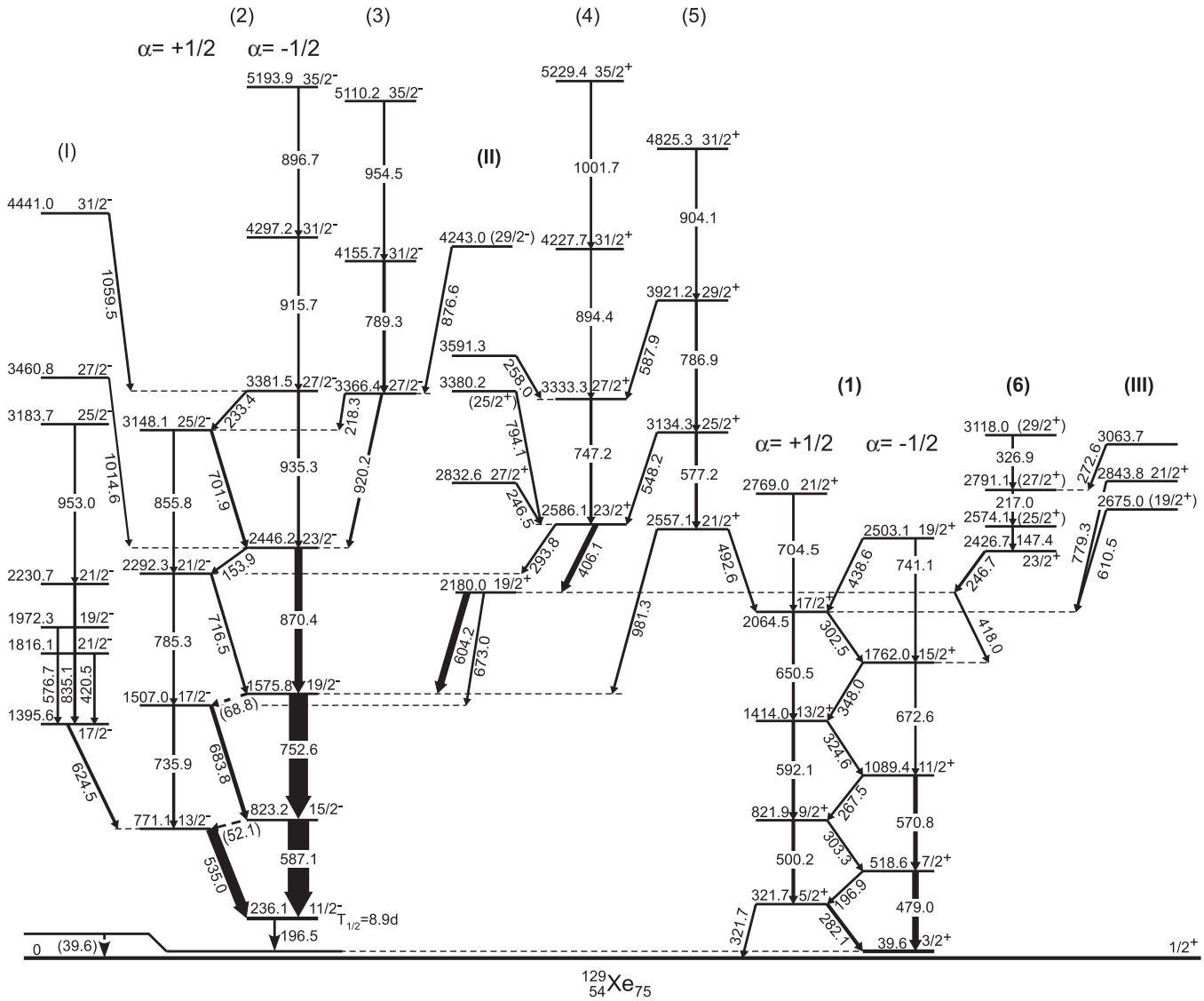

FIG. 1. Level scheme of ^{129}Xe obtained in the present work. Energies are in keV.

parity (I^π) up to the $17/2^+$ state for the $\alpha = +1/2$ signature component and to the $15/2^+$ state for the $\alpha = -1/2$ one, along with those linking γ transitions below the $17/2^+$ state. However, in Ref. [24], the two signature components in this band were considered as two separate band structures based on $3/2^+$ and $5/2^+$ states, respectively. In this work, we regard them as two signature components of band (1) based on the $3/2^+$ state according to the general rotational band character. Then this band is extended up to $21/2^+$ at the 2769.0-keV level for the $\alpha = +1/2$ signature component and to $19/2^+$ at the 2503.1-keV level for the $\alpha = -1/2$ one in the present work. Four γ transitions, at 741.1, 704.5, 302.5, and 438.6 keV, are also newly identified in this band. The 2433.5-keV level reported in [24], along with the transition at 671.2 keV, is not observed in the present work. For the negative-parity band, (2), based on the $11/2^-$ state, it was identified to $23/2^-$ at the 2466.2-keV level for the $\alpha = -1/2$ signature component in Ref. [23]. Above that, we find three new levels, at 3381.5 keV ($27/2^-$), 4297.2 keV ($31/2^-$), and 5193.9 keV ($35/2^-$), along with three transitions, at 935.3, 915.7, and 896.7 keV, in this signature component. Although three levels, at 771.1 keV ($13/2^-$), 1507.7 keV ($17/2^-$), and 2292.3 keV ($21/2^-$), were identified in Ref. [23], they were not formed in the $\alpha = +1/2$ signature component of band (2). We identified a new level at 3148.1 keV ($25/2^-$) and new transitions at 735.9, 785.3, and 855.8 keV, so that the four levels 771.1, 1507.0, 2292.3, 3148.1 keV form the $\alpha = +1/2$ signature component of band (2). The level at 2586.1 keV reported in Ref. [23] is assigned as the band head of band (4) in this work. In addition, several new levels and transitions in clusters (I)–(III) as well as new linking transitions between the bands and the cluster levels have been identified. The two levels at 1395.6 and 1972.3 keV, with cascade depopulation transitions at 624.5 and 576.7 keV, reported in Ref. [23], are reassigned as single-particle levels in cluster (I). The spin and parity of the levels at 1395.6 keV ($17/2^-$), 1816 keV ($21/2^-$), and 1972.3 keV ($19/2^-$) are reassigned in comparison with Ref. [24]. The new assignments are supported by the $E2$ polarity of the 420.5- and 624.5-keV γ transitions, while the transition at 576.7 is of $M1/E2$ polarity, which is not changed under the new assignments. In high-spin states, four collective bands, (3)–(6), based on 3366.4-, 2586.1-, 2557.1-, and 2426.7-keV levels, respectively, are identified for the first time in this work. A summary of the γ-ray energies, relative intensities, DCO ratios, multipolarities, and I^π assignments as well as the corresponding level energies of ^{129}Xe are listed in Table I. The DCO ratios are obtained with the formula $R_{\rm DCO} = \frac{I_{\gamma_1}^{\theta_1}(\text{gate on } \gamma_2 \text{ at } \theta_2)}{I_{\gamma_1}^{\theta_2}(\text{gate on } \gamma_2 \text{ at } \theta_1)}$, where θ_1 stands for the non-90° detectors while θ_2 represents the 90° detectors. With gating on stretched quadrupole transitions assigned in Refs. [23] and [24], the $R_{\rm DCO}$ ratio obtained is around 0.6 for a known stretched quadrupole γ transition and greater than 1 for a known pure stretched $\Delta I = 1$ γ transition, with a few exceptions at 604.2 and 673.0 keV for unclear reasons. The multipolarities are shown in parentheses if not confirmed by the DCO ratios, while for some existing transitions without DCO ratios, the multipolarities are taken from [23]. The I^π's for the levels are assigned or tentatively assigned according to previous results [23,24], the DCO ratios of the γ transitions obtained in the present work, and the level spacings inside the bands. The I^π's of the 2586.4-keV level [the band-head level of band (4)] and the 2180.0-keV level were assigned as $23/2^-$ and $19/2^-$, respectively, in Refs. [23] and [24]. According to the transition pattern and observed DCO ratios in the present work, we assignedthese two levels I^π's of $23/2^+$ and $19/2^+$, respectively. The 2586.1-keV level is de-excited to the 2292.3-keV ($21/2^-$) level in band (2) through the 293.8-keV transition and to the 2180.0-keV ($19/2^+$) level through the 406.1-keV transition, respectively. The latter level is then depopulated through the 604.2- and 673.0-keV transitions to the 1575.8-keV ($19/2^-$) and 1507.0-keV ($17/2^-$) levels in band (2) and through the 418-keV transition to the 1762.0-keV (15^+) level in band (1), respectively. Notably the 2180.0-keV level and its strongest depopulation transition, at 604.2 keV, were found in Ref. [23] and assigned as quasiparticle levels. But we change its parity due to the presence of the 418-keV transition, which is of $E2$ polarity instead of $M2$ polarity according to our DCO and intensity data. Meanwhile, the reassignment of the parity of the 2180.0-keV level from negative to positive changes the polarity of the 604.2-keV γ transition from $M1$ to $E1$, which, in principle, causes no problem. As an example, we present some coincidence γ spectra for ^{129}Xe. Figure 2 shows the coincidence γ spectra obtained by gating on the 587.1-keV transition. The corresponding γ transitions above the 823.2-keV level can be clearly seen. Figure 3 presents the coincidence γ spectra to visualize the occurrence of the transitions in bands (1) and (6). In Fig. 3(a), with gating on the 479.0-keV γ transition, all the corresponding γ transitions above the 518.6-keV level in band (1) and the linking γ transitions in other bands can be seen. In Fig. 3(b), all the γ transitions in band (6) can be seen with gating on the 246.7-keV γ transition.

III. DISCUSSION

We start the discussion of the band structures with bands (1) and (2) in ^{129}Xe. In previous studies, the I^π's of the band-head level at 39.6 keV in band (1) were assigned as $3/2^+$ from the β^+ decay of ^{129}Cs and further applied to interpret the multipolarities of the γ rays decaying to the 39.6-keV level and the $1/2^+$ ground state from the higher-lying levels [23,24,27]. For band (2), the isomer of the 236.1-keV ($11/2^-$) band-head level was initially observed in Ref. [28] and the I^π was confirmed through the observation of a 40-keV Auger electron in a ^{129}Xe^m sample [29]. A strong cascade of γ transitions based on this negative-parity state was reported in Ref. [23]. Based on these I^π assignments, the configuration could be further understood by Nilsson level scheme calculations. Figure 4 presents the Nilsson diagram for neutrons and protons of ^{129}Xe calculated in this work. Given that ^{129}Xe is an odd-N nucleus with $N = 75$, one can inspect the Nilsson diagram of the neutron in Fig. 4(a). At a given deformation at about $\beta_2 = 0.1$–0.2 (see the calculated TRS results in Fig. 7), the neutron Fermi surface is near the $3/2^+[402]$ and $11/2^-[505]$ orbits, which lie slightly above the $9/2^-[514]$. According to the systematic character of the $3/2^+$

TABLE I. Energies, relative intensities, DCO ratios, multipolarities, and spin and parity (I^{π}) assignments of the γ transitions and levels in ^{129}Xe. Asterisks denote γ transitions newly identified in this work.

E_γ (keV)	Intensity (%)	E_i (keV)	E_f (keV)	Assignment	R_{DCO}	Multipolarity
(39.6)		39.6	0	$3/2^+ \rightarrow 1/2^+$		
(52.1)*		823.2	771.1	$15/2^- \rightarrow 13/2^-$		$(M1/E2)$
(68.8)*		1575.8	1507.0	$19/2^- \rightarrow 17/2^-$		$(M1/E2)$
147.4*	1.2(1)	2574.1	2426.7	$(25/2^+) \rightarrow 23/2^+$		$(M1/E2)$
153.9*	0.56(20)	2446.2	2292.3	$23/2^- \rightarrow 21/2^-$		$(M1/E2)$
196.5		236.1	39.6	$11/2^- \rightarrow 3/2^+$		$M4$[23]
196.9	1.46(1)	518.6	321.7	$7/2^+ \rightarrow 5/2^+$		$M1/E2$[23]
217.0*	0.69(7)	2791.1	2574.1	$(27/2^+) \rightarrow (25/2^+)$		$(M1/E2)$
218.3*	0.21(8)	3366.4	3148.1	$27/2^- \rightarrow 25/2^-$		
233.4*	0.44(10)	3381.5	3148.1	$27/2^- \rightarrow 25/2^-$		$(M1/E2)$
246.5*	1.69(1)	2832.6	2586.1	$27/2^+ \rightarrow 23/2^+$	0.73(27)	$E2$
246.7*	2.50(1)	2426.7	2180.0	$23/2^- \rightarrow 19/2^-$	0.72(21)	$E2$
258.0*	0.38(1)	3591.3	3333.3	$\text{—} \rightarrow 27/2^+$		
267.5	0.85(1)	1089.4	821.9	$11/2^+ \rightarrow 9/2^+$		$(M1/E2)$
272.6*	0.13(5)	3063.7	2791.1	$\text{—} \rightarrow 27/2^-$		
282.1	12.7(1)	321.7	39.6	$5/2^+ \rightarrow 3/2^+$		$M1/E2$[23]
293.8*	0.98(9)	2586.1	2292.3	$23/2^+ \rightarrow 21/2^-$	1.23(6)	$E1$
302.5*	0.12(3)	2064.5	1762.0	$17/2^+ \rightarrow 15/2^+$		$(M1/E2)$
303.3	2.21(1)	821.9	518.6	$9/2^+ \rightarrow 7/2^+$	0.82(13)	$M1/E2$
321.7	1.5(1)	321.7	0	$5/2^+ \rightarrow 1/2^+$		$E2$[23]
324.6*	0.93(1)	1414.0	1089.4	$13/2^+ \rightarrow 11/2^+$	1.02(27)	$M1/E2$
326.9*	0.14(5)	3118.0	2791.1	$(29/2^+) \rightarrow (27/2^+)$	1.32(75)	$M1/E2$
348.0*	0.55(1)	1762.0	1414.0	$15/2^+ \rightarrow 13/2^+$	1.21(51)	$M1/E2$
406.1	22.4(1)	2586.1	2180.0	$23/2^+ \rightarrow 19/2^+$	0.44(12)	$E2$
418.0*	0.34(7)	2180.0	1762.0	$19/2^+ \rightarrow 15/2^+$	0.47(15)	$E2$
420.5	1.78(2)	1816.1	1395.6	$21/2^- \rightarrow 17/2^-$	0.34(12)	$E2$
438.6*	0.17(1)	2503.1	2064.5	$19/2^+ \rightarrow 17/2^+$		$(M1/E2)$
479.0	26.7(1)	518.6	39.6	$7/2^+ \rightarrow 3/2^+$		$E2$[23]
492.6*	1.65(2)	2557.1	2064.5	$21/2^+ \rightarrow 17/2^+$	0.79(30)	$E2$
500.2	12.3(8)	821.9	321.7	$9/2^+ \rightarrow 5/2^+$	0.79(15)	$E2$
535.0	46.7(49)	771.1	236.1	$13/2^- \rightarrow 11/2^-$		$M1/E2$[23]
548.2*	2.12(1)	3134.3	2586.1	$25/2^+ \rightarrow 23/2^+$	1.87(48)	$M1/E2$
570.8	16.5(3)	1089.4	518.6	$11/2^+ \rightarrow 7/2^+$	0.54(6)	$E2$
576.7	2.23(3)	1972.3	1395.6	$19/2^- \rightarrow 17/2^-$	0.87(27)	$M1/E2$
577.2*	3.9(1)	3134.3	2557.1	$25/2^+ \rightarrow 21/2^+$	0.82(24)	$E2$
587.1	100(9)	823.2	236.1	$15/2^- \rightarrow 11/2^-$		$E2$[23]
587.9*		3921.2	3333.3	$29/2^+ \rightarrow 27/2^+$		$(M1/E2)$
592.1	11.5(1)	1414.0	821.9	$13/2^+ \rightarrow 9/2^+$	0.60(15)	$E2$
604.2	29.1(1)	2180.0	1575.8	$(19/2^+) \rightarrow 19/2^-$	0.67(6)	$(E1)$
610.5*	2.35(3)	2675.0	2064.5	$(19/2^+) \rightarrow 17/2^+$	1.68(84)	$(M1/E2)$
624.5	10.0(1)	1395.6	771.1	$17/2^- \rightarrow 13/2^-$	0.49(6)	$E2$
650.5	8.71(5)	2064.5	1414.0	$17/2^+ \rightarrow 13/2^+$	0.49(12)	$E2$
672.6	5.9(22)	1762.0	1089.4	$15/2^+ \rightarrow 11/2^+$	0.59(6)	$E2$
673.0*	5.9(1)	2180.0	1507.0	$19/2^+ \rightarrow 17/2^-$	0.90(20)	$(E1)$
683.8	15.2(1)	1507.0	823.2	$17/2^- \rightarrow 15/2^-$	1.88(21)	$M1/E2$
701.9*	3.68(1)	3148.1	2446.2	$25/2^- \rightarrow 23/2^-$	1.66(39)	$M1/E2$
704.5*	3.33(4)	2769.0	2064.5	$21/2^+ \rightarrow 17/2^+$	0.62(57)	$E2$
716.5	8.2(1)	2292.3	1575.8	$21/2^- \rightarrow 19/2^-$	1.55(21)	$M1/E2$
735.9*	9.1(1)	1507.0	771.1	$17/2^- \rightarrow 13/2^-$	0.21(3)	$E2$
741.1*	0.78(1)	2503.1	2064.5	$19/2^+ \rightarrow 15/2^+$	0.54(15)	$E2$
747.2*	8.88(3)	3333.3	2586.1	$27/2^+ \rightarrow 23/2^+$	0.76(12)	$E2$
752.6	88.2(2)	1575.8	823.2	$19/2^- \rightarrow 15/2^-$	0.54(3)	$E2$
779.3*	1.05(2)	2843.8	2064.5	$21/2^+ \rightarrow 17/2^+$	0.37(12)	$E2$
785.3*	6.45(3)	2292.3	1507.0	$21/2^- \rightarrow 17/2^-$	0.48(24)	$E2$
786.9*	2.6(1)	3921.2	3134.3	$29/2^+ \rightarrow 25/2^+$	0.55(12)	$E2$
789.3*	4.8(1)	4155.7	3366.4	$31/2^- \rightarrow 27/2^-$	0.56(12)	$E2$
794.1*	2.07(1)	3380.2	2586.1	$(25/2^+) \rightarrow 23/2^+$	2.02(60)	$(M1/E2)$

TABLE I. (*Continued.*)

E_γ (keV)	Intensity (%)	E_i (keV)	E_f (keV)	Assignment	R_{DCO}	Multipolarity
835.1*	3.14(4)	2230.7	1395.6	$21/2^- \rightarrow 17/2^-$	0.32(12)	$E2$
855.8*	1.67(3)	3148.1	2292.3	$25/2^- \rightarrow 21/2^-$	0.32(27)	$E2$
870.4	33.44(1)	2446.2	1575.8	$23/2^- \rightarrow 19/2^-$	0.51(3)	$E2$
876.6*	0.85(2)	4243.0	3366.4	$(29/2^-) \rightarrow 27/2^-$	3.12(72)	$(M1/E2)$
894.4*	4.21(4)	4227.7	3333.3	$31/2^+ \rightarrow 27/2^+$	0.31(18)	$E2$
896.7*	0.54(6)	5193.9	4297.2	$35/2^- \rightarrow 31/2^-$	0.55(36)	$E2$
904.1*	1.6(1)	4825.3	3921.2	$31/2^+ \rightarrow 29/2^+$	0.76(30)	$E2$
915.7*	2.42(3)	4297.2	3381.5	$31/2^- \rightarrow 27/2^-$	0.76(24)	$E2$
920.2*	8.87(2)	3366.4	2446.2	$27/2^- \rightarrow 23/2^-$	0.63(9)	$E2$
935.3*	8.85(2)	3381.5	2446.2	$27/2^- \rightarrow 23/2^-$	0.50(9)	$E2$
953.0	0.86(7)	3183.7	2230.7	$25/2^- \rightarrow 21/2^-$	0.67(51)	$E2$
954.5*	1.6(1)	5110.2	4155.7	$35/2^- \rightarrow 31/2^-$	0.57(24)	$E2$
981.3*	6.9(1)	2557.1	1575.8	$21/2^+ \rightarrow 19/2^-$	2.35(48)	$E1$
1001.7*	1.1(1)	5229.4	4227.7	$35/2^+ \rightarrow 31/2^+$	0.33(27)	$E2$
1014.6*	3.98(1)	3460.8	2446.2	$27/2^- \rightarrow 23/2^-$	0.83(24)	$E2$
1059.5*	2.42(2)	4441.0	3381.5	$31/2^- \rightarrow 27/2^-$	0.48(27)	$E2$

[27] and $11/2^-$ [30–33] states, the positive-parity band, (1), can be assigned as the $\nu d_{3/2}3/2^+[402]$ configuration with the 39.6-keV $(3/2^+)$ band-head level, and the negative-parity band (2) can be assigned as the $\nu h_{11/2}\,11/2^-[505]$ configuration with the 236.1-keV $(11/2^-)$ band-head level. We note here that these Nilsson states are derived from axial shapes and zero rotations. If the nucleus is triaxially deformed, however, there might be considerable mixing with low-K components. These configuration assignments are also consistent with our one-quasiparticle plus triaxial rotor model (PRM) calculations (see later discussion). It should be mentioned that there is a tentative $9/2^-$ state found for the $N = 75$ isotones [34], which implies that the assignment as the [514]9/2 orbital is also likely. However, we have not observed a $9/2^-$ level in band (2).

The ^{129}Xe nucleus is located in the $A \approx 130$ transitional region characterized by a smooth shape transition from prolate to oblate or triaxial collective motion. In odd-N nuclei, the largest deformation is near the midshell, i.e., $N = 66$. Light nuclei below the midshell will approximately possess a prolate deformation, while above the middle shell, the deformation will be developed to oblate via the triaxial region, characterized by an experimentally detectable signal like signature splitting. It has been shown that at low spins, either the negative-parity

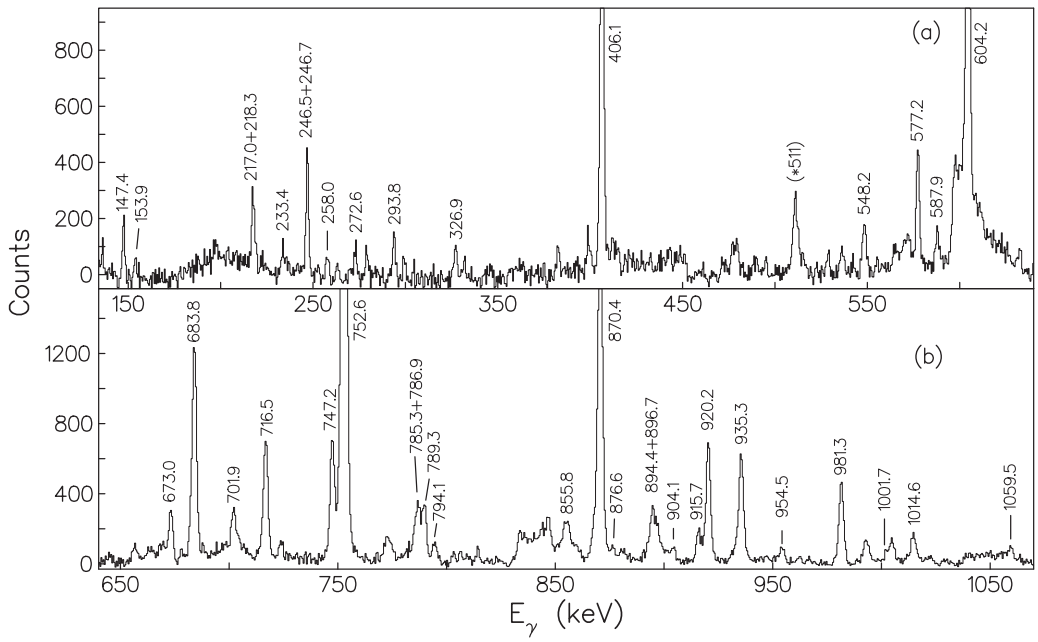

FIG. 2. Coincidence γ-ray spectra obtained by gating on the 587.1-keV γ-transition in ^{129}Xe. Energy intervals of γ rays extend (a) from 130 to 640 keV and (b) from 640 to 1070 keV.

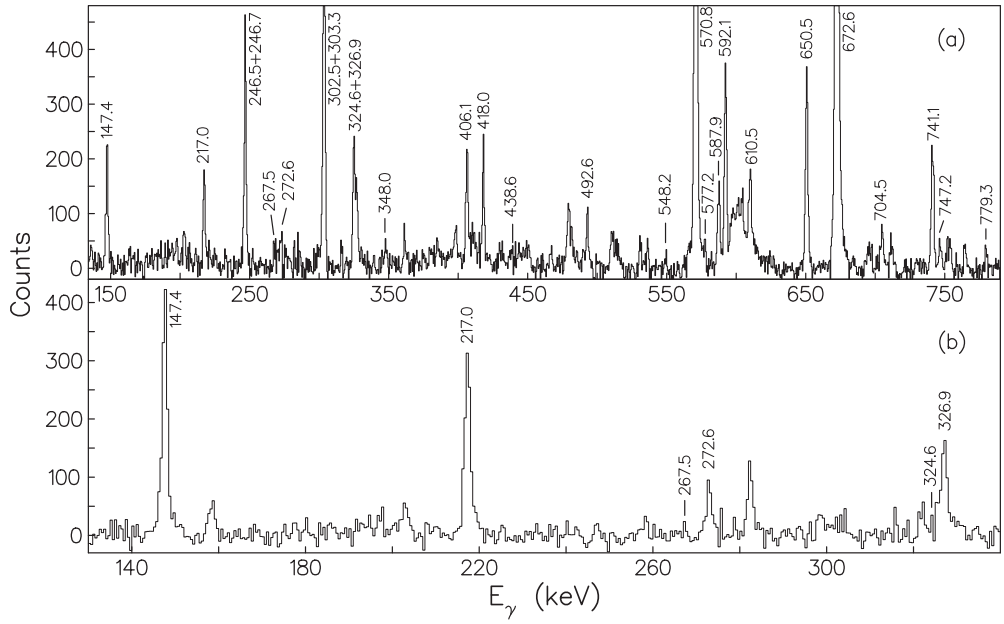

FIG. 3. Portion coincidence γ-ray spectra obtained by gating on (a) the 479.0-keV and (b) the 246.7-keV γ transitions in ^{129}Xe.

band or the positive-parity band [23] in the ^{129}Xe nucleus fits well in the systematics. Figure 5 compares the levels for the positive-parity band, (1), in ^{129}Xe from the present work with those in odd-A ^{131,133}Xe [27]. A smooth evolution is shown; level energies with the same spin increase slightly with increasing neutron number. In Fig. 6, we compare the levels for the negative-parity band, (2), in ^{129}Xe from the present work with those in odd-A ^{125}Xe [35] and ^{127}Xe [36]. Again, the systematics is evident. For the ^{125,127}Xe isotopes, although the negative-parity bands are based on the $9/2^-$ level originating from the $h_{11/2}9/2^-[514]$ configuration, if the energy is normalized to the $11/2^-$ level, as shown in Fig. 6, one can see that the energy gap in either the favored signature or the unfavored signature increases slightly with increasing neutron number. The agreement of the behavior of the level structures in ^{129}Xe with the systematics for the two bands indicates a similar structural character for these isotopes.

To gain a general understanding of the structural characteristics of ^{129}Xe in bands (1) and (2), TRS calculations have been performed within the framework of the cranked shell model [37–39]. In this approach, the total energy of a nucleus can be written as the sum of a macroscopic term and a microscopic term. The macroscopic term is approximated by the standard liquid drop model. The microscopic term is related to the single-particle properties of the nucleons near the Fermi surface, which are evaluated in an average potential well represented by a non–axially deformed Woods-Saxon potential [40]. The calculation is performed in the deformation space (β_2, γ, β_4). The pairing correlation is treated by the Lipkin-Nogami approach, in which the particle number is conserved approximately [41,42]. The pairing energy is calculated considering both the monopole and the doubly stretched quadrupole interactions. The ground-state deformation is taken as the value corresponding to the minimum total energy. The minimum TRS indicates the favored deformation under

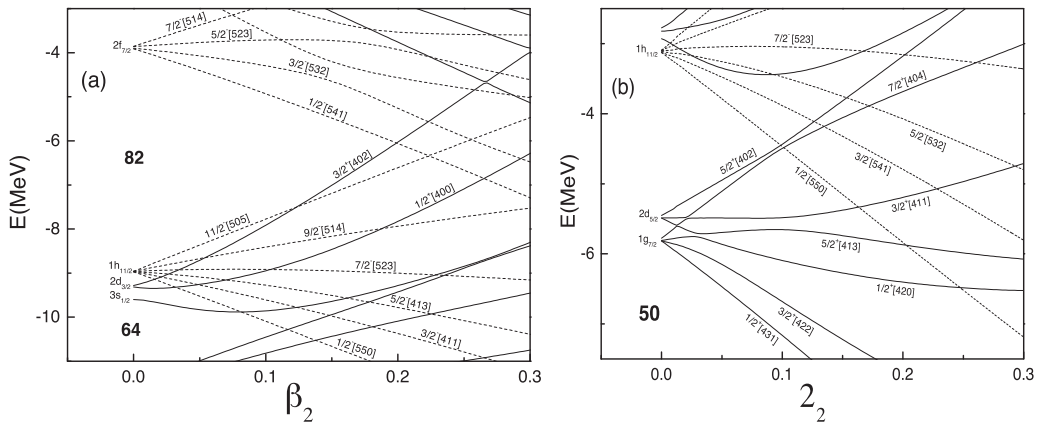

FIG. 4. Partial Nilsson diagram for (a) neutrons and (b) protons of ^{129}Xe.

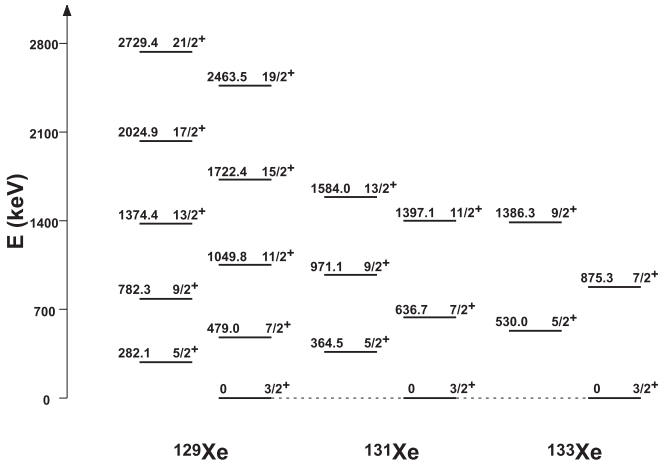

FIG. 5. Systematic comparison of the levels of the positive band, (1), in ^{129}Xe with those in ^{131}Xe and ^{133}Xe.

the given conditions. Figure 7 presents the TRS distribution at $\hbar\omega = 0$. It is shown that the minimum appears at $\beta_2 = 0.15$, $\beta_4 = 0.003$, and $\gamma = -26.3^\circ$, which suggests that the ^{129}Xe nucleus has a triaxial deformation in the ground state. Here the parameters β and γ are defined in the Lund convention [43]. On the other hand, the potential surface exhibits a rather flat valley over a wide range of γ values, varying from -30° to 30° and near -90°, indicating an unstable nuclear shape which usually exhibits γ softness or vibration motion as discussed in Ref. [24]. This is consistent with the picture of the coexisting prolate-triaxial-oblate minima commonly existing on TRS surfaces in odd-N Xe isotopes [8].

A staggering parameter $S(I)$ with the form of [44]

$$S(I) = E(I) - [E(I+1) + E(I-1)]/2 \qquad (1)$$

has been derived experimentally for bands (1) and (2) in ^{129}Xe and is plotted in Fig. 8 as a function of the doubled spin values $2I$. Filled (open) symbols denote the $\alpha = +1/2$ ($\alpha = -1/2$) signature components. For the positive-parity band, (1), the signature splitting is at the magnitude of 100 keV and a signature inversion appears at $2I = 13\,\hbar$. Generally, the signature splitting should be related to the γ deformation. For the negative-parity band, (2), the signature splitting reaches approximately 500 keV, indicating the occurrence of a maximized triaxiality, consistent with the TRS surface calculation in Fig. 7, where a minimum at $\gamma = -26.3^\circ$ is observed. Even though the [505]11/2 orbital is assigned to the negative-parity band, (2), according to the Nilsson states obtained from the axial shape at zero frequency, with such large triaxiality, there might be considerable mixing with low-K components, leading to the large signature splitting.

Figure 9 presents the experimental $B(M1)/B(E2)$ as a function of the spin. It is shown that the ratio is much smaller than unity for band (1) but is situated at a higher level, increasing with the spin, in band (2). The difference between band (1) and band (2) can be qualitatively understood within the semiclassical formula of Dönau and Frauendorf derived within the particle-rotor framework [45,46]. In that formula,

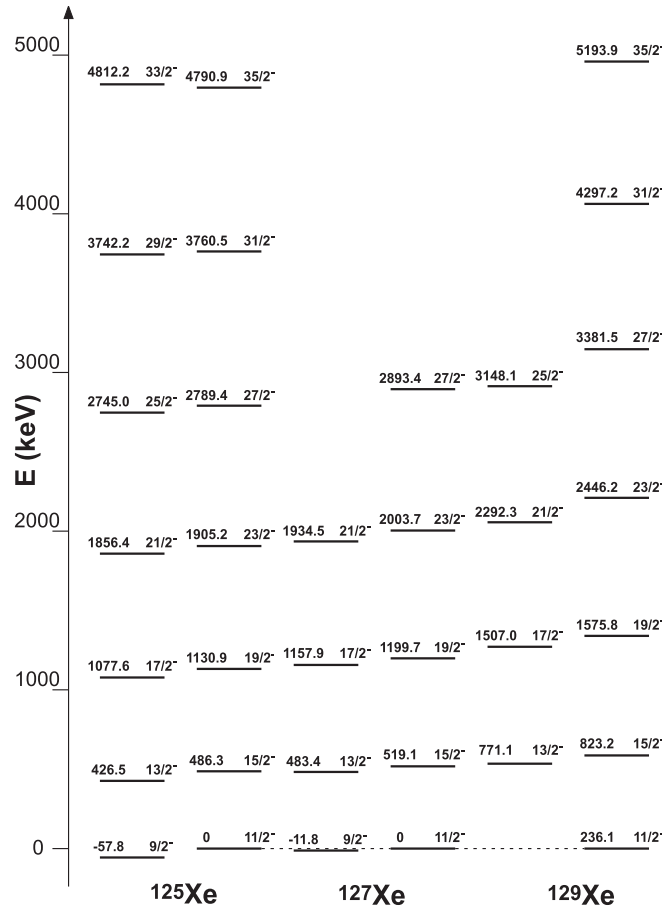

FIG. 6. Systematic comparison of the levels of the negative band, (2), in ^{129}Xe with those in ^{125}Xe and ^{127}Xe.

the ratio is proportional to $[K(g - g_R)^2]/[Q_0^2 \cos^2(\gamma + 30^\circ)]$, where Q_0 is the quadrupole moment, K is the K value of the quasiparticle causing the signature splitting, g is the g factor, and g_R is the rotational g factor, usually taken as equal to Z/A. As for bands (1) and (2), the relevant quasiparticle orbitals are $d_{3/2}$ and $h_{11/2}$, for which the g factors are $3.8q/5$ and $-3.8q/11$, respectively, where $q \approx 0.6$ is the quenching factor. The $B(M1)/B(E2)$ ratio for band (1) is pretty low in relation to the fact that g and $-g_R$ roughly cancel each other. The ratio for band (2) is much higher since both g and $-g_R$ contribute to the same phase.

Figure 10 presents the kinetic moment of inertia $J^{(1)}$ of bands (1) and (2) in ^{129}Xe versus the rotational frequency $\hbar\omega$. Here the moment of inertia and the rotational frequency are obtained from $J_1 = I_x/\hbar\omega$, where $I_x = \sqrt{(I_a + 1/2)^2 - K^2}$, $I_a = (I_i + I_f)/2$, and $\hbar\omega = (E_i - E_f)/[I_x(I_i) - I_x(I_f)]$. For the positive-parity band, (1), $J^{(1)}$ increases nearly linearly with the frequency for both signature components, which may suggest the occurrence of a gradual rotation alignment of two high-j $h_{11/2}$ neutrons at a frequency lower than 0.3 MeV. For the negative-parity band, (2), a backbending is found for the $\alpha = -1/2$ signature component at approximately $\hbar\omega = 0.45$ MeV. To understand the backbending property observed in ^{129}Xe, we have carried out cranked shell model

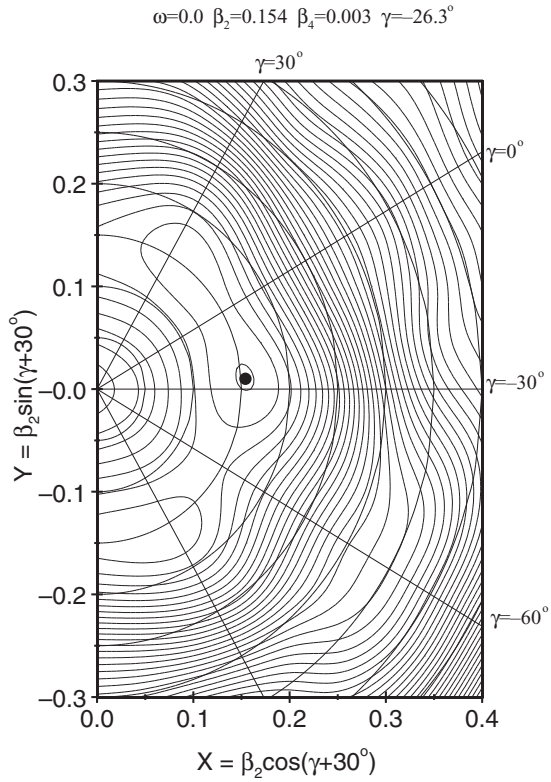

FIG. 7. TRS calculation for ^{129}Xe at $\hbar\omega = 0.0$ MeV.

calculations with a modified oscillator potential, which is described in detail by Bengtsson *et al.* [47] and Frauendorf *et al.* [37,38]. The parameters used in the calculations were $\beta_2 = 0.154$, $\beta_4 = 0.003$, and $\gamma = -26.3°$. These parameters were obtained from the minima of the above TRS calculations. The other parameters were taken as standard. The calculated quasiparticle energies (Routhians) for ^{129}Xe are presented in Fig. 11(a) for protons and Fig. 11(b) for neutrons, respectively. The calculations predict that a backbending caused by the alignments of two $h_{11/2}$ protons occurs at $\hbar\omega = 0.5$ MeV,

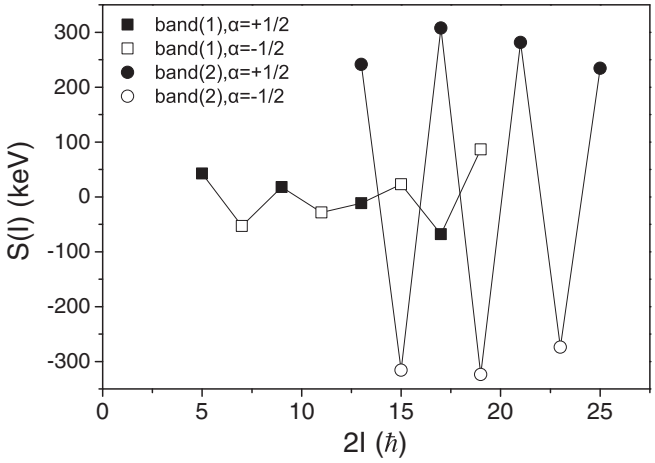

FIG. 8. The energy staggering parameter $S(I)$ vs the spin I for bands (1) and (2) in ^{129}Xe.

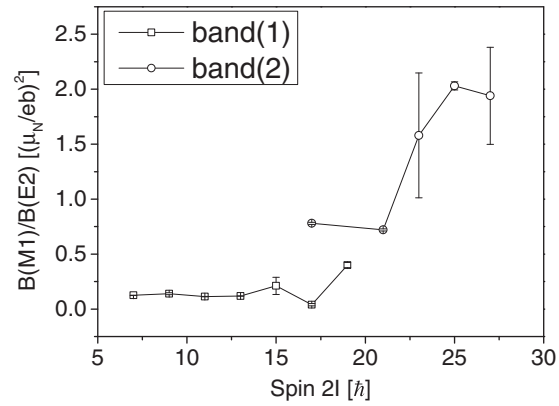

FIG. 9. The $B(M1)/B(E2)$ ratio as a function of the spin I for bands (1) and (2) in ^{129}Xe.

in rough agreement with the experimental value in band (2). For quasineutron levels, on the other hand, the alignment occurring at $\hbar\omega = 0.27$ MeV, which is much lower than the experimental backbending value in band (2), is possibly a signature of the gradual rotation alignment of two neutrons on the high-j orbital, manifesting as a gradual increase in the momentum of inertia in band (1). Thus, it is suggested that the backbending in the negative-parity band, (2), in ^{129}Xe is associated with the alignments of two $\pi h_{11/2}$ protons. A similar backbending frequency caused by the proton alignments has also been observed in odd-N isotopes in the Xe-Ba-Ce region [8].

To further investigate the deformation effects on the rotational structure built on the quasineutron configuration in bands (1) and (2), the one-quasiparticle plus triaxial rotor model calculation [48] has been performed with and without consideration of the triaxial deformation. The standard parameter set of the Nilsson model is used [49] and the momentum of inertia is adjusted to get a reasonable description of the bulk properties of the bands. The deformation parameters β_2 and γ are taken from the TRS predictions. Figure 12 shows the PRM calculation of the energy levels for the negative-parity

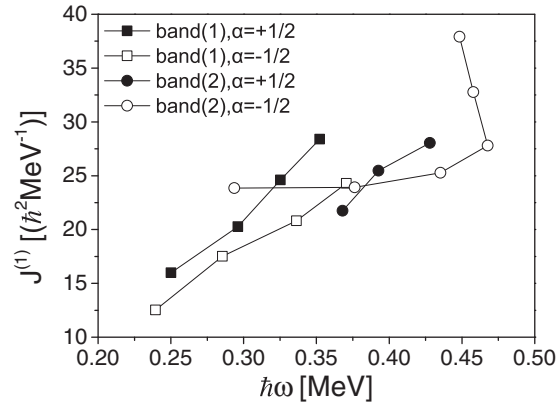

FIG. 10. Plots of the moments of inertia $J^{(1)}$ as a function of the rotational frequency $\hbar\omega$ for bands (1) and (2). Filled and open symbols correspond to the $\alpha = +1/2$ and $\alpha = -1/2$ signatures, respectively.

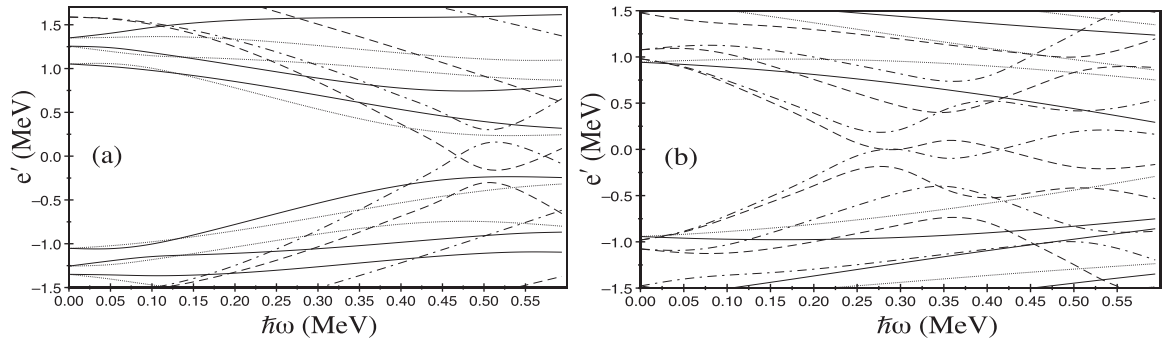

FIG. 11. Plot of the calculated Routhians for (a) quasiprotons and (b) quasineutrons vs the rotational frequency $\hbar\omega$ in ^{129}Xe. The parity and signature (π,α) of the levels are as follows: (+,+1/2) solid lines, (+,−1/2) dotted lines, (−, + 1/2) dot-dashed lines, and (−, −1/2) dashed lines.

band, (2); results with a single triaxiality parameter, $\gamma = -30^\circ$, are presented. It is shown that the experimental structure is well reproduced by the calculation. Thus the negative-parity band, (2), can be regarded as a triaxially deformed band. For the positive-parity band, (1), a single γ is not sufficient to interpret the data over the whole range of the spin. Figure 13 presents exemplarily the PRM calculations at $\gamma = 0^\circ$, -15°, and -30°. It is shown that the calculation at $\gamma = -15^\circ$ exhibits some features qualitatively similar to the data, but quantitative reproduction of the level structure is unlikely to be achieved with a single γ. Indeed, for the lower levels, the level scheme and the decay properties in the positive-parity band could

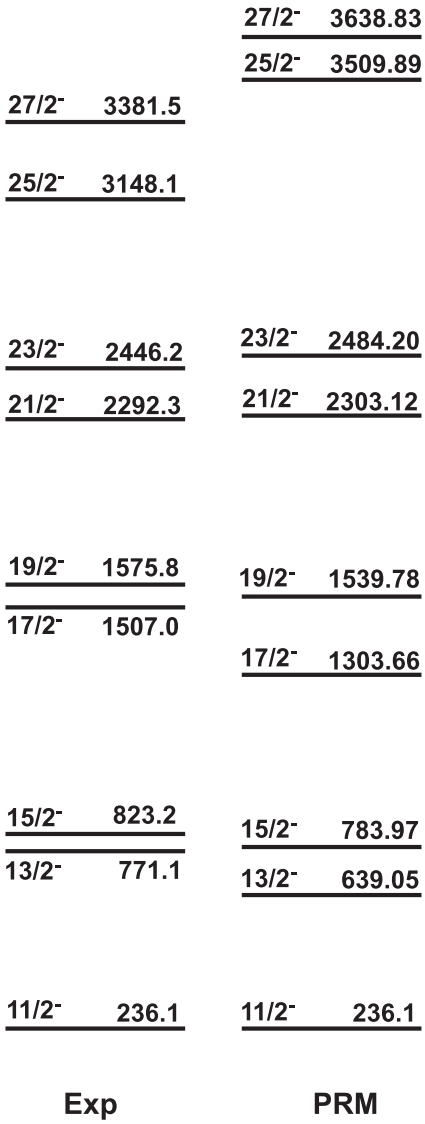

FIG. 12. Comparison of the levels between experimental data and PRM calculations for the negative-parity band, (2), in ^{129}Xe with $\gamma = -30^\circ$.

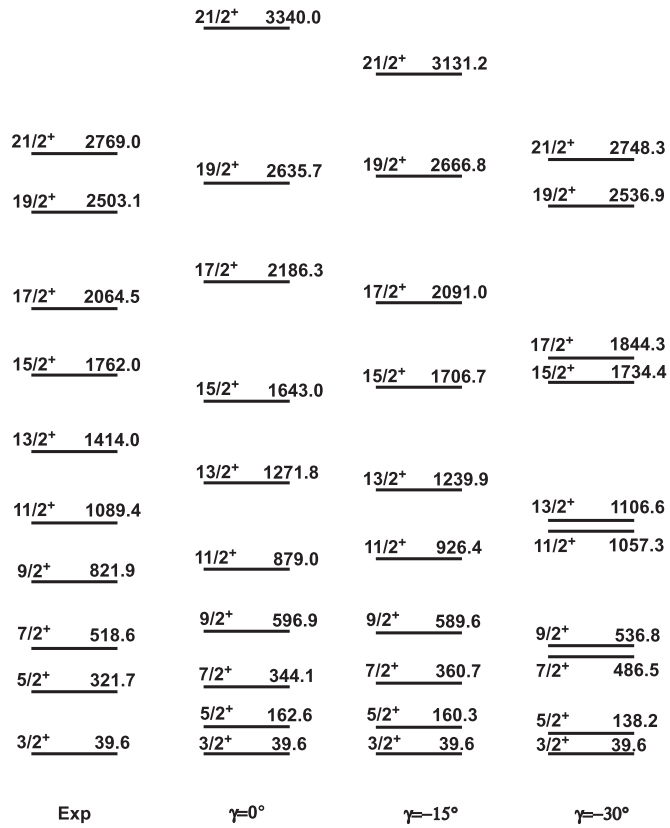

FIG. 13. Comparison of the levels between experimental data and PRM calculations for the positive-parity band, (1), in ^{129}Xe with different γ deformations.

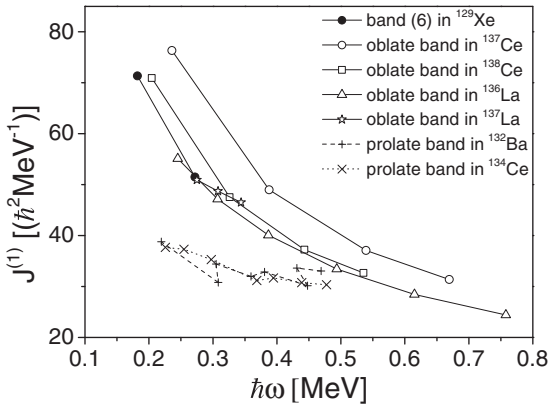

FIG. 14. Comparison of the moments of inertia $J^{(1)}$ of band (6) in ^{129}Xe with the oblate bands in ^{137}Ce , ^{138}Ce , ^{136}La, and ^{137}La and the prolate bands in ^{132}Ba and ^{134}Ce vs the rotational frequency $\hbar\omega$.

be interpreted with a particle plus core model assuming a vibration-type core excitation, but reproduction of the data was not achieved using a triaxial rotor with a common set of parameters [23]. This suggests that the polarization effect of an odd particle on a soft core comes into play. Similar γ softness was also found in the ^{128}Xe nucleus [19]. Comparison to the PRM calculations infers that the positive-parity band, (1), and the negative-parity band, (2), have different shapes. Further theoretic studies on the positive-parity band, (1), are necessary. On the other hand, the calculations show that the positive-parity band, (1), and the negative band, (2), indeed originate from the $\nu d_{3/2}3/2^+[402]$ and $\nu h_{11/2}\,11/2^-[505]$ Nilsson orbitals, respectively.

In high-spin states, bands (3)–(5) consist of $\Delta I = 2E2$ transitions. They are considered as decoupled bands. They were also observed in the odd-odd ^{134,136}Pr [50,51] and ^{138,140}Pm [16,52] and odd-A ^{139}Pr [15] and ^{141}Pm [53] in this region. The origin of this kind of structure is that the configuration for the valence neutron or valence proton should include a low-Ω orbital. So the large signature splitting between favored and unfavored components may occur [51]. In this work, only one signature constituent is observed. According to the calculated Nilsson diagram in Fig. 4, the possible configurations for the decoupled bands, (3), (4), and (5), in ^{129}Xe are suggested to be $\pi[g_{7/2}]^2 \otimes \nu f_{7/2}1/2^-[541]$, $\pi g_{7/2} \cdot h_{11/2} \otimes \nu f_{7/2}1/2^-[541]$, and $\pi d_{5/2} \cdot g_{7/2} \otimes \nu d_{3/2}1/2^+[400]$, respectively.

Band (6) in ^{129}Xe only consists of $\Delta I = 1\,M1$ transitions inside the band. It shows features similar to those of the other known oblate bands in the $A \approx 130$ region: (a) strong $\Delta I = 1$ transitions relative to the $E2$ crossover transitions, (b) no signature splitting, and (c) moments of inertia different from those of prolate bands. A plot of the moments of inertia $J^{(1)}$ of band (6) in ^{129}Xe along with those of the oblate bands in ^{137}Ce [54], ^{138}Ce [55], ^{136}La [10], and ^{137}La [11] and the prolate bands in ^{132}Ba [56] and ^{134}Ce [57] versus the rotational frequency $\hbar\omega$ is shown in Fig. 14. Generally, the $J^{(1)}$ values of prolate bands are less than those of oblate bands [9,12,55]. One can see that the $J^{(1)}$ values of band (6) in ^{129}Xe show behavior similar to that of the oblate bands in the neighboring nuclei, but different from that of the prolate bands. The cranked shell model calculations show that the alignment of a pair of $h_{11/2}$ protons favors a prolate shape with $\gamma \approx 0^\circ$ and the alignment of a pair of $h_{11/2}$ neutrons favors an oblate shape with $\gamma \approx -60^\circ$ [17]. Band (6) is probably of three-quasiparticle configurations. It is tentatively assigned as the $\nu d_{3/2} \cdot [h_{11/2}]^2$ configuration, for which the oblate band observed in ^{129}Xe should be caused by a pair of the $h_{11/2}$ neutron alignments in high-spin states.

The characteristics of single-particle levels in clusters (I)—(III) are not clear; further studies are required to understand them.

IV. SUMMARY

The level structures in ^{129}Xe have been reinvestigated and the level scheme extended. At lower spins, the two signature components are extended and put together to form a complete positive-parity band, based on the $3/2^+$ state with the $\nu d_{3/2}3/2^+[402]$ configuration. For the negative-parity band, based on the $11/2^-$ state, the $\alpha = -1/2$ signature component is newly established. The $\alpha = +1/2$ and the $\alpha = -1/2$ signature components are combined to form a complete band with the $\nu h_{11/2}11/2^-[505]$ configuration, and this band is expanded with spin and parity up to $35/2^-$. A backbending has been observed in the negative-parity band, which originates from the alignments of two $h_{11/2}$ protons according to the cranked shell model calculations. TRS and PRM calculations have been conducted to reveal the deformation properties of ^{129}Xe via the band structures. The negative-parity band structure is predicted by PRM calculations assuming a triaxial deformation with $\gamma \approx -30^\circ$, while the positive-parity band seems to show, differently, γ softness, since the calculations using a single γ deformation cannot reproduce the data. In high-spin states, three decoupled bands and an oblate band are identified. It is demonstrated that the oblate deformation driving effect is caused by a pair of $\nu h_{11/2}$ neutrons in high-spin states in ^{129}Xe following the systematics in the $A \approx 130$ mass region. The systematics and other characteristics of these bands have been discussed.

ACKNOWLEDGMENTS

The work at Tsinghua University was supported by the National Science Foundation of China (NSFC) under Grant Nos. 11175095, 11205112, and 11375094, by the Tsinghua University Initiative Scientific Research Program, and by the Special Program of the Higher Education Science Foundation under Grant No. 2010000211007. C.Q. was supported by the Swedish Research Council (VR) under Grant Nos. 621-2010-3694, 621-2012-3805, and 621-2013-4323. The calculations were performed on resources provided by the Swedish National Infrastructure for Computing (SNIC) at PDC, KTH, Stockholm. The authors wish to thank the staff of the tandem accelerator group at China Institute of Atomic Energy for providing the heavy-ion beam and the target of a high quality.

[1] N. V. Zamfir and R. F. Casten, Phys. Lett. B **260**, 265 (1991).
[2] H. J. Li, Z. G. Xiao, S. J. Zhu, E. Y. Yeoh, Y. X. Liu, Y. Sun, Z. Zhang, R. S. Wang, H. Yi, W. H. Yan, Q. Xu, X. G. Wu, C. Y. He, Y. Zheng, G. S. Li, C. B. Li, H. W. Li, J. J. Liu, S. P. Hu, J. L. Wang, and S. H. Yao, Phys. Rev. C **87**, 057303 (2013).
[3] S. W. Ødegård, G. B. Hagemann, D. R. Jensen, M. Bergström, B. Herskind, G. Sletten, S. Törmänen, J. N. Wilson, P. O. Tjøm, I. Hamamoto, K. Spohr, H. Hubel, A. Görgen, G. Schönwasser, A. Bracco, S. Leoni, A. Maj, C. M. Petrache, P. Bednarczyk, and D. Curien, Phys. Rev. Lett. **86**, 5866 (2001).
[4] R. F. Casten, E. A. McCutchan, N. V. Zamfir, C. W. Beausang, and J. Y. Zhang, Phys. Rev. C **67**, 064306 (2003).
[5] S. P. Hu *et al.*, Phys. Lett. B **732**, 59 (2014).
[6] Y. S. Chen, S. Frauendorf, and G. A. Leander, Phys. Rev. C **28**, 2437 (1983).
[7] H. J. Li, Z. G. Xiao, S. J. Zhu, M. Patial, C. Qi, B. Cederwall, Z. Zhang, R. S. Wang, H. Yi, W. H. Yan, W. J. Cheng, Y. Huang, L. M. Lyu, Y. Zhang, X. G. Wu, C. Y. He, Y. Zheng, G. S. Li, C. B. Li, H. W. Li, J. J. Liu, P. W. Luo, S. P. Hu, J. L. Wang, and Y. H. Wu, Phys. Rev. C **91**, 054314 (2015).
[8] A. Granderath *et al.*, Nucl. Phys. A **597**, 427 (1996).
[9] E. S. Paul, C. W. Beausang, D. B. Fossan, R. Ma, W. F. Piel Jr.,, N. Xu, L. Hildingsson, and G. A. Leander, Phys. Rev. Lett. **58**, 984 (1987).
[10] S. J. Zhu *et al.*, Eur. Phys. J. A **24**, 199 (2005).
[11] M. L. Li *et al.*, Eur. Phys. J. A **28**, 1 (2006).
[12] E. S. Paul, D. B. Fossan, Y. Liang, R. Ma, and N. Xu, Phys. Rev. C **40**, 1255 (1989).
[13] N. Xu, C. W. Beausang, R. Ma, E. S. Paul, W. F. Piel, D. B. Fossan, and L. Hildingsson, Phys. Rev. C **39**, 1799 (1989).
[14] M. L. Li, S. J. Zhu, X. L. Che, Y. N. Yu, Y. J. Chen, H. B. Ding, L. H. Zhu, X. G. Wu, S. X. Wen, C. Y. He, X. Z. Cui, and Y. Liu, Phys. Rev. C **75**, 034304 (2007).
[15] E. Y. Yeoh, S. J. Zhu, J. G. Wang, Z. G. Xiao, M. Zhang, W. H. Yan, R. S. Wang, Q. Xu, X. G. Wu, C. Y. He, G. S. Li, Y. Zheng, C. B. Li, X. P. Cao, S. P. Hu, S. H. Yao, and B. B. Yu, Phys. Rev. C **85**, 064322 (2012).
[16] H. J. Li *et al.*, Eur. Phys. J. A **51**, 60 (2015).
[17] Q. Xu, S. J. Zhu, X. L. Che, J. G. Wang, H. B. Ding, L. Gu, L. H. Zhu, X. G. Wu,Y Liu, C. Y. He, and G. S. Li, Phys. Rev. C **78**, 034310 (2008).
[18] R. Wyss *et al.*, Nucl. Phys. A **505**, 337 (1989).
[19] J. N. Orce, A. M. Bruce, A. Emmanouilidis, A. P. Byrne, G. D. Dracoulis, T. Kibedi, M. Caamano, H. El-Masri, C. J. Pearson, Z. Podolyak, P. D. Stevenson, P. M. Walker, F. R. Xu, D. M. Cullen, and C. Wheldon, Phys. Rev. C **74**, 034318 (2006).
[20] G. Marest, R. Haroutunian, I. Berkes, M. Meyer, M. Rots, J. De Raedt, H. Van de Voorde, H. Oonis, and R. Coussement, Phys. Rev. C **10**, 402 (1974).
[21] R. A. Meyer, F. F. Momyer, J. H. Landrum, E. A. Henry, R. P. Yaffe, and W. B. Walters, Phys. Rev. C **14**, 1152 (1976).
[22] I. Rezanka, A. Kerek, A. Luukko, and C.J. Herrlander, Nucl. Phys. A **141**, 130 (1970).
[23] H. Helppi, J. Hattula, A. Luukko, and M. Jääskeläinen, Nucl. Phys. A **357**, 333 (1981).
[24] Z. Zhao *et al.*, Z. Phys. A **331**, 113 (1988).
[25] K. S. Krane, R. M. Steffen, and R. M. Wheeler, Nucl. Data Tables **11**, 351 (1973).
[26] D. C. Radford, Nucl. Instrum. Meth. A **361**, 297 (1995).
[27] T. Lonnroth, J. Kumpulainen, and C. Tuokko, Phys. Scripta **27**, 228 (1983).
[28] I. Bergström, Nature **167**, 634 (1951).
[29] S. Thulin and I. Bergstrom, Phys. Rev. **85**, 1055 (1952).
[30] A. Luukko, J. Hattula, H. Helppi, and O. Knuuttila, Nucl. Phys. A **357**, 319 (1981).
[31] J. Gizon A. Gizon, and J. Meyer-Ter-Vehn, Nucl. Phys. A **277**, 464 (1977).
[32] J. Gizon and A. Gizon, Z. Phys. A **281**, 99 (1977).
[33] H. Helppi J. Hattula, and A. Luukko, Nucl. Phys. A **332**, 183 (1979).
[34] J. Timar, Z. Elekes, and B. Singh, Nucl. Data Sheets **121**, 143 (2014).
[35] C. B. Moon, C. S. Lee, T. Komatsubara, Y. Sasaki, and K. Furuno, Phys. Rev. C **76**, 067301 (2007).
[36] W. Urban T. Morek, Ch. Droste, B. Kotliński, J. Srebrny, J.Wrzesiński, and J. Styczeń, Z. Phys. A **320**, 327 (1985).
[37] S. Frauendorf, Phys. Lett. B **100**, 219 (1981).
[38] S. Frauendorf and F. R. May, Phys. Lett. B **125**, 245 (1983).
[39] F. R. Xu, W. Satuła, and R. Wyss, Nucl. Phys. A **669**, 119 (2000).
[40] J. Dudek, Z. Szymanski, T. Werner, A. Faessler, and C. Lima, Phys. Rev. C **26**, 1712 (1982).
[41] H. Pradhan, Y. Nogami, and J. Law, Nucl. Phys. A **201**, 357 (1973).
[42] W. Satuła, R. Wyss, and P. Magierski, Nucl. Phys. A **578**, 45 (1994).
[43] G. Andersson, S. E. Larsson, G. Leander, P. Möller, S. G. Nilsson, I. Ragnarsson, and S. Åberg, Nucl. Phys. A **268**, 205 (1976).
[44] A. J. Kreiner, M. A. J. Mariscotti, C. Baktash, E. derMateosian, and P. Thieberger, Phys. Rev. C **23**, 748 (1981).
[45] F. Dönau and S. Frauendorf, in *Proceedings of the Conference on High Angular Momentum Properties of Nuclei, Oak Ridge*, edited by N. R. Johnson (Harwood, New York, 1983), p. 143.
[46] F. Dönau, Nucl. Phys. A **471**, 469 (1987).
[47] R. Bengtsson and S. Frauendorf, Nucl. Phys. A **327**, 139 (1979).
[48] S. E. Larsson, G. Leander, and I. Ragnarsson, Nucl. Phys. A **307**, 189 (1978).
[49] T Bengtsson and I Ragnarsson, Nucl. Phys. A **436**, 14 (1985).
[50] C. M. Petrache D. Bazzaccoa, S. Lunardia, C. Rossi Alvareza, G. de Angelisb, M. De Polib, D. Bucurescuc, C.A. Urc, P.B. Semmesd, and R. Wysse, Nucl. Phys. A **597**, 106 (1996).
[51] C. M. Petrache *et al.*, Nucl. Phys. A **603**, 50 (1996).
[52] J. G. Wang *et al.*, J. Phys. G: Nucl. Part. Phys. **37**, 125107 (2010).
[53] L. Gu, S. J. Zhu, J. G. Wang, E. Y. Yeoh, Z. G. Xiao, S. Q. Zhang, J. Meng, M. Zhang, Y. Liu, H. B. Ding, Q. Xu, L. H. Zhu, X. G. Wu, C. Y. He, G. S. Li, L. L. Wang, Y. Zheng, and B. Zhang, Phys. Rev. C **83**, 064303 (2011).
[54] S. J. Zhu, L. Y. Zhu, M. Li, C. Y. Gan, M. Sakhaee, L. M. Yang, R. Q. Xu, Z. Zhang, Z. Jiang, G. L. Long, S. X. Wen, X. G. Wu, and X. A. Liu, Phys. Rev. C **62**, 044310 (2000).
[55] S. J. Zhu *et al.*, Chin. Phys. Lett. **16**, 635 (1999).
[56] S. Juutinen, S. Tormanen, P. Ahonen, M. Carpenter, C. Fahlander, J. Gascon, R. Julin, A. Lampinen, T. Lonnroth, J. Nyberg, A. Pakkanen, M. Piiparinen, K. Schiffer, P. Simecek, G. Sletten, and A. Virtanen, Phys. Rev. C **52**, 2946 (1995).
[57] S. J. Zhu *et al.*, High Energy Phys. Nucl. Phys. **29**, 130 (2005) [in Chinese].